# Polylactide/cellulose nanocrystals: the *in situ* polymerization approach to improved nanocomposites

Stefano Gazzotti,[a,b] Hermes Farina,[a,b] Giordano Lesma,[a,b] Riccardo Rampazzo,[a] Luciano Piergiovanni,[b,c]
Marco Aldo Ortenzi,[a,b]* Alessandra Silvani[a,b]

[a.] *Dipartimento di Chimica, Università degli Studi di Milano, via Golgi 19, Milano, 20133, Italy.*
[b.] *CRC Materiali Polimerici "LaMPo", Dipartimento di Chimica, Università degli Studi di Milano, via Golgi 19, Milano, 20133, Italy.*
[c.] *DeFENS, Department of Food, Environmental and Nutritional Sciences, Università degli Studi di Milano, via Celoria 2, Milano, 20133, Italy.*
*\*E-mail: marco.ortenzi@unimi.it*

The *in situ* polymerization of L-lactide in the presence of various amounts of cellulose nanocrystals (CNC) is described. CNC was prepared efficiently by acidic hydrolysis of cotton linters. Molecular weight, morphology, thermal, mechanical and crystallization properties of the PLA-CNC nanocomposites were evaluated. From size-exclusion chromatography (SEC) analysis, the actual occurrence of chemical bond between CNC and PLA can be assessed. The effect of CNC has been evaluated through differential scanning calorimetry (DSC) analysis, which highlights the probable formation of α' crystals in the obtained materials. More importantly, from thermogravimetric analysis (TGA) a marked improvement in thermal stability of nanocomposites has been demonstrated, with respect to standard PLA and to previously described PLA-CNC blends. Nanocomposites show also an improvement in rheological properties with respect to standard PLA. In particular, storage modulus greatly increases, indicating a reinforcing effect of CNC. The described *in situ* synthetic methodology allows an optimal compatibilization between the two entities (PLA and CNC), facing one of the major problems inherent to the preparation of nanocomposites. It leads furthermore to remarkably improved thermal and rheological properties of the obtained materials.

## Introduction

In recent years environmental awareness has been focused onto the replacing of traditional plastics based on petrochemical resources with alternative, more eco-friendly materials. Among them, poly(lactic acid), shortly PLA, is one of the most attractive to researchers and industry,[1] because of its good biodegradability and availability from renewable sources, such as starch and sugar beet.[2] The growing attention towards this thermoplastic polymer comes from both its outstanding properties, such as the good optical and elastic behavior and the excellent melt-processability, and, at the same time, from its cost competitiveness, also with respect to more traditional, not biodegradable polyesters such as PET.[3,4] For all these reasons, nowadays PLA has gained commercial significance and greatly increased its market, especially for what regards packaging and disposables applications.

However, PLA suffers from a lot of drawbacks that strongly limit possibilities for its wide application in many sectors. Indeed, it is endowed with low thermal and mechanical stability upon processing conditions, scarce flexibility and poor barrier properties. All these characteristics place it behind commonly used plastics, for instance for food packaging applications.[5]

Among possible alternatives to overcome some of these limitations, the preparation of nanocomposites has emerged as the most promising suitable solution.[6] In nanocomposites, the surface area/volume ratio of employed reinforcement additives is crucial to the enhancement of material properties. Indeed, as dimensions reach the nanometer level, interactions at phase interfaces become largely improved, bringing nanocomposites to exhibit properties not expected with larger scale particulate reinforcements. A lot of different additives can in principle be used as nanofillers. Among others, carbon nanotubes,[7,8] montmorillonite[9,10] and nanosilica[11,12] have been studied, with satisfactory achievements, in the design of PLA nanocomposites.

Aiming to produce fully organic bionanocomposites, cellulose nanocrystals (CNC) have recently emerged as a kind of biocompatible, biodegradable and renewable additive that could be dispersed into the PLA polymer matrix for the preparation of high performance blends. CNC are acquiring more and more interest in several

54 fields of application thanks to unique chemical and mechanical properties. They are rod-like particles with
55 extremely high aspect ratio, high Young modulus, low density and high surface area. CNC can be extracted
56 from almost every cellulose source, with different extraction methods properly described in literature.[13, 14,]
57 [15] Basically, they all rely onto the disruption of amorphous regions in cellulose fibers that are more susceptible
58 of reaction (acid hydrolysis or oxidation reactions mainly), while preserving crystalline regions that can be
59 isolated. Alongside the cited outstanding physical properties, the carbohydrate nature of these crystals
60 ensures interesting chemical properties. The presence of a great quantity of free hydroxyl groups, primary
61 and secondary, on CNC surface can be both a drawback and an advantage when blends with PLA are
62 prepared. In fact, at a first glance, the high polarity of CNC clashes with the relatively apolar nature of PLA,
63 resulting in dispersion problems that can seriously impact the properties of the obtained composite material.
64 On the other side, however, the high quantity of reactive moieties on CNC opens to a lot of possible chemical
65 derivatizations, that can be exploited in order to confer better compatibility with the polymer matrix.
66 Various preparation methods have been developed to obtain biocomposites by blending PLA with different
67 amounts of CNC.[16, 17] In some of these biocomposites, CNC have been preventively chemically modified in
68 order to improve the interfacial adhesion with the polymer matrix.[18, 19] One effective method for chemical
69 modification of CNC is to grow polymers directly off their surface, using the "grafting-from" approach.[20] By
70 this way, short PLA oligomers have been successfully grafted from CNC using a ring-opening polymerization
71 (ROP) protocol, affording PLA-bearing CNC, which were then blended with PLA.[21, 22, 23] Quite recently, a
72 further enhancement of compatibilization of CNC with the PLA matrix was described by Dhar and co-workers,
73 who employed a reactive extrusion process in order to graft PLA chains onto CNC through a radical reaction.[24]
74 In PLA-CNC nanocomposites obtained via compounding, thermal degradation of both PLA and CNC during
75 extrusion is an unsolved issue. Only small improvements in thermal stability of the obtained materials are
76 reported in few cases, especially when reactive extrusion is carried out in the presence of chain extenders
77 and radical initiators.[25]
78 On the basis of our related experience on preparation of PLA nanocomposites containing nanosilica (NS)[11] or
79 modified montmorillonite (MMT)[9], we looked at PLA-CNC nanocomposites via the *in situ* polymerization of
80 L-lactide in the presence of various amounts of CNC.
81 It is well established that *in situ* polymerization in the presence of fillers provides distinct advantages when
82 compared to other nanocomposite synthesis techniques, appearing more appropriate in providing excellent
83 dispersion of the nanoparticles, which should have a greater impact on achievable properties. The *in situ*
84 polymerization technique has been recently applied for the preparation of various PLA nanocomposites,
85 incorporating for instance $TiO_2$[26] or MMT fillers.[27] Marked improvements in thermal properties and
86 crystallinity of the resultant composites were obtained, compared to those of the standard polymers.
87 To the best of our knowledge, no *in situ* polymerization strategies employing CNC have been described for
88 the preparation of PLA nanocomposites. In this study, the *in situ* polymerization of L-lactide was performed
89 with different loading ratios of CNC, prepared by acidic hydrolysis of cotton linters. The protocol exploits the
90 alcoholic moieties of CNC as initiators in ring opening polymerization reaction of L-lactide. Molecular weight,
91 morphology, thermal, mechanical and crystallization properties of the obtained nanocomposites were
92 evaluated.
93
94 **Experimental**
95
96 **Synthesis of Cellulose Nanocrystals**
97 Cellulose nanocrystals were obtained by acidic hydrolysis, as described in literature.[15] Triturated cotton
98 linters were slowly added to a preheated solution of 64 % w/w sulfuric acid. The ratio fiber : sulfuric acid was
99 1 : 17.5 g/mL. The cotton hydrolysis was performed under vigorous stirring at 45 °C for 45 min. After this
100 period, the solution was diluted with 10 times-volume deionized water in order to stop the acidic hydrolysis.
101 The suspension was then centrifuged at least 5 times at 10000 rpm for 20 minutes each round. The
102 precipitated solid was repeatedly rinsed and centrifuged with deionized water. In order to remove the acid
103 excess, the centrifuged solution was put into a dialysis tubes immersed in deionized water for 3 days. The
104 suspension was then sonicated repeatedly (0.7 cycles of 15 min at 70 % output) to create cellulose crystals
105 of colloidal dimensions. In order to complex any stray ions, an ion-exchange resin was put into the dispersion
106 for 24 hours at room temperature. After resin removal, the suspension was filtered under vacuum with a

107 Whatman glass microfiber filter to remove the largest cellulose-fiber agglomerates. Finally, the dispersion
108 was lyophilized using a lab lyophilizator, obtaining a white-dried powder.
109
110 **Synthesis of PLA**
111 PLA was synthesized from L-lactide in bulk according to the following procedure. L-lactide (25 g) and tin
112 octanoate (0.3 % w/w on lactide), added as catalyst, were introduced in a 250 mL three necked round
113 bottomed flask. Slow nitrogen flow was used to ensure the presence of inert atmosphere during
114 polymerization reaction. Mechanical stirring was provided (40 rpm). Reaction was conducted in a closed oven
115 at 180 °C for 2 hours. At the end of the reaction, the polymer was left cooling overnight under nitrogen
116 atmosphere.
117
118 **Synthesis of PLA-CNC nanocomposites**
119 Nanocomposites were synthesized by *in situ* polymerization, from L-lactide in bulk according to the following
120 procedure. CNC in different quantities, from 0.125 grams – used to synthesize PLA0.5 – to 1.250 grams –
121 used to synthesize PLA5 (see **Table 1**), were put in a three-necked round bottomed flask and dispersed in 50
122 mL of acetone under vigorous stirring and ultrasound treatment. This procedure ensures the disaggregation
123 of the lyophilized CNC fluffy mass into single crystals.
124 25 g of L-lactide were then added and left under stirring until complete dissolution. Acetone was then
125 evaporated using nitrogen flux. The reaction mixture was then heated to 70 °C under vacuum in a closed
126 oven for 2 hours in order to remove any residual moisture. After this drying step, reaction was performed
127 following the procedure described for the synthesis of PLA. Five nanocomposites samples (PLA0.5, PLA2,
128 PLA2.5, PLA3, PLA5) were prepared varying the percentage of employed CNC (see Table 1).
129

| Sample | Cellulose Nanocrystals | |
|---|---|---|
| | (%wt) | (g) |
| PLA | 0 | 0 |
| PLA0.5 | 0.5 | 0.125 |
| PLA2 | 2 | 0.500 |
| PLA2.5 | 2.5 | 0.625 |
| PLA3 | 3 | 0.750 |
| PLA5 | 5 | 1.250 |

**Table 1:** Samples synthesized and CNC relative and absolute quantities.

143 **Characterization**
144
145 **Size Exclusion Chromatography (SEC).** The effect of CNC on the molecular weight of obtained
146 nanocomposites was evaluated using a SEC system having Waters 1515 Isocratic HPLC pump and a four
147 Waters Styragel columns' set (HR3-HR4-HR5-HR2) with an UV detector Waters 2487 Dual $\lambda$ Absorbance
148 Detector set at 230 nm using a flow rate of 1 mL/min and 60$\mu$L as injection volume. Samples were prepared
149 dissolving 50 mg of polymer in 1 mL of anhydrous $CH_2Cl_2$ and filtering the solution on 0.45 $\mu$m filters. Given
150 the relatively high loading, a check was performed using lower concentration of polymer (5mg/mL), in order
151 to verify that no column overloading could be observed. Anyway higher loadings were preferred as UV signal
152 of PLA is relatively weak.
153 Molecular weight data are expressed in polystyrene (PS) equivalents. The calibration was built using
154 monodispersed PS standards having the following nominal peak molecular weight
155 (Mp) and molecular weight distribution (D): Mp=1,600,000 Da (D≤1.13), Mp=1,150,000 Da (D≤1.09),
156 Mp=900,000 Da (D≤1.06), Mp=400,000 Da (D≤1.06), Mp=200,000 Da (D≤1.05), Mp= 90,000 Da (D≤1.04),
157 Mp=50,400 Da (D=1.03), Mp=30,000 Da (D=1.06), Mp=17,800 Da (D=1.03), Mp=9,730 Da (D=1.03), Mp=5,460
158 Da (D=1.03), Mp=2,032 Da (D=1.06), Mp=1,241 Da (D=1.07), Mp=906 Da (D=1.12), Mp=478 Da (D=1.22); Ethyl
159 benzene (molecular weight=106 g/mol). For all analyses, 1,2-dichlorobenzene was used as internal reference.

160
**Differential Scanning Calorimetry (DSC).** DSC analyses were conducted using a Mettler Toledo DSC1, on samples weighting from 5 to 10 mg each. Melting and crystallization temperatures were measured using the following temperature cycles:

1. Heating from 25 °C to 200 °C at 10 °C/min;
2. 5 min isotherm at 200 °C;
3. Cooling from 200 °C to 25 °C at 10 °C/min;
4. 2 min isotherm at 25 °C;
5. Heating from 25 °C to 70 °C at 10 °C/min;
6. Heating from 70 °C to 200 °C at 5 °C/min.

The first two cycles were run to eliminate residual internal stresses deriving from the synthesis. Glass transition temperature ($T_g$), cold crystallization temperature ($T_{cc}$) and melting temperature ($T_m$) were determined. The lower heating rate in the last cycle (i.e. cycle number 6) was used in order to better separate the cold crystallization and melting peaks.

**Thermogravimetric Analysis (TGA).** TGA were performed using a TGA 4000 Perkin Elmer instrument; tests were conducted in air on samples weighting from 5 to 10 mg each, with a program that provides a single heating cycle from 30 °C to 800 °C at 10 °C/min.

**Rheological Curves.** Rheological analyses, conducted using frequency sweep experiments, were performed with a Physica MCR 300 rotational rheometer with a parallel plate geometry (diameter = 25 mm, distance between plates = 1 mm). Linear viscoelastic regimes of neat PLA and PLA nanocomposites were studied; strain was set equal to 5% and curves of complex viscosity as function of frequency were recorded, taking 30 points ranging from 100 Hz to 0.1 Hz with a logarithmic progression, at 190 °C.

**Wide Angle X-Ray Scattering (WAXS).** Wide Angle X-Ray Scattering (WAXS) experiments were performed using a Rigaku DMAX-II diffractometer. Diffraction patterns were obtained in the range 5° < 2θ < 60° with Cu-Kα radiation (λ = 1.5405 $\mathring{A}$) under the following conditions: 40 kV, 40 mA, step width 0.02°, time per step 2 sec, divergence slit 0.25°, Soller slit 0.04 rad and antiscatter slit 0.5°. X-Ray patterns are normalized on the main peak.

**Films Casting.** Films for WAXS analyses were obtained from a chloroform solution; 10 grams of polymer were dissolved into 50 grams of $CHCl_3$. The solution was cast on a glass surface and the solvent was evaporated at room temperature and pressure overnight. Film thickness was determined by Nikon eclipse ME600 optical microscope with Nikon digital camera light DS-Fil, software NIS-Element BR, and magnification 50x, and it was in the range 60-90 μm.

**Transmission Electron Microscopy (TEM) analysis.** For the analysis of CNC, drops of aqueous dispersions of CNC (1 wt%) were deposited on carbon-coated electron microscope grids, negatively stained with uranyl acetate and allowed to dry. For the analysis of nanocomposites, a representative sample was chosen: PLA5 was cut with a microtome and the slices obtained were negatively stained with uranyl acetate. Samples were analyzed with a Hitachi Jeol-10084 TEM operated at an accelerating voltage of 80 kV.

**Fourier Transform Infrared Spectroscopy (FT-IR).** FT-IR Spectrometer (Spectrum 100, PerkinElmer) with an attenuated total reflection (ATR) was used to register spectra for PLA sample, all nanocomposites and CNC alone. FT-IR spectra of PLA, CNC and PLA5 are shown in the Supporting Information file. Significant peaks for PLA/Nanocomposites: 1747 cm$^{-1}$ (C=O stretching), 1000-1200cm$^{-1}$ (C-O stretching). Significant peaks for CNC: 3335 cm$^{-1}$ (-OH stretching), 1032 cm$^{-1}$ (C-O stretching).

**$^1$H NMR analyses.** $^1$H NMR spectra for PLA sample and nanocomposites were registered with a Bruker Ultrashield 400 MHz. The chemical shifts are reported in ppm and referred to TMS as internal standard. All samples were prepared by dissolving 6-8 mg of polymer into 1 mL of $CDCl_3$. Spectra of PLA and PLA5 are

212 shown in the Supporting Information file. Peaks attribution for the $^1$H NMR (400 MHz, CDCl$_3$): δ 5.18 (H-1, q,
213 *J* = 4 Hz), 1.60 (H-2, d, J = 4 Hz).
214
215 **Results and discussion**
216
217 **Synthesis of PLA-CNC nanocomposites.**
218 A schematic representation of the *in situ* synthesis of PLA-CNC nanocomposites is reported in **Scheme 1**. The
219 product of the reaction is likely to be a complex mixture of species, with both free PLA chains and PLA-grafted
220 CNC. Free PLA shows a molecular weight distribution from SEC analyses. CNC can be characterized by
221 different degrees of functionalization.
222
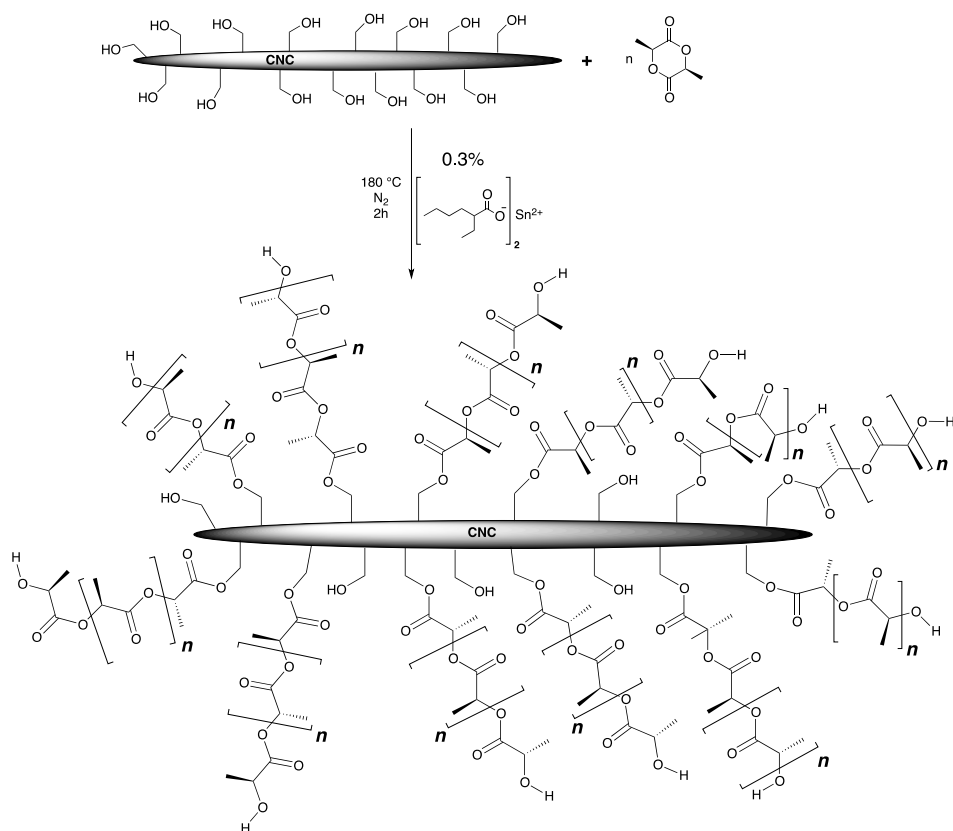


**Scheme 1:** schematic representation of the *in situ* synthesis of PLA-CNC.

225 Synthesis provided semi-crystalline materials characterized by an increasing brownish shade as the
226 concentration of nanocrystals increased. The polymers are homogeneous and no CNC are visible, indicating
227 an optimal dispersion within the nanocomposite.
228
229 **Size exclusion chromatography (SEC)**
230 SEC curves were obtained for all samples. As described in experimental section, samples were filtered on
231 0.45 *μm* filters before the analysis, therefore SEC data refer only to the polymer present in solution.
232 In **Figure 1** selected SEC graphs (PLA, PLA0.5 and PLA3) are reported. Curves have been normalized with
233 respect to the peak relative to the most abundant polymeric species for all samples. As expected, PLA SEC

234 curve shows only a peak at low retention time, related to the polymer. The peaks between 2400 secs and
235 2700 secs are attributable to low molecular weight species and residual monomer. PLA0.5 and PLA3 samples,
236 containing 0.5 wt.% and 3 wt.% of CNC respectively, show two additional peaks at very low retention times
237 (around 1100 secs and 1200 secs). It should be noted that such peaks get more intense as the wt.% of CNC
238 increases. Given the presence of additional peaks, $\overline{M_n}$ and $\overline{M_w}$ values for CNC-containing nanocomposites
239 cannot be considered reliable. For this reason, only $M_p$ values are presented in **Table 2**, where $M_p$ refers to
240 the peak around 1400-1700 secs. $M_p$ can be defined as the mass value for the most abundant species in
241 chromatogram. Observing the trend moving from PLA to PLA0.5 and PLA3 graphs, it can be stated that the
242 peak around 1400-1700 secs is attributable to "standard" PLA chains, straightly obtained through ROP of
243 lactide. Hydroxyl groups present as moisture in the polymerization apparatus and the small quantity of lactic
244 acid present together with lactide likely promote such conventional process.

245 However, employing CNC in the *in situ* polymerization process, covalently bound CNC are also obtained, as
246 CNC can act as initiators through their hydroxyl groups, affording various possible CNC containing polymeric
247 species.

248 From **Figure 1**, it could be noted that higher wt.% of CNC present in the feed leads to a decrease of molecular
249 weight of standard PLA chains. This datum strongly supports the hypothesis that free OH groups on CNC's
250 surface participate in the ROP of lactide. In fact, as the CNC's concentration increases in the feed, more
251 initiators will be actually present, leading to shorter chains. The additional peaks which are present in the
252 SEC-graphs of PLA0.5 and PLA3 at very high hydrodynamic volumes are likely attributable to polymeric
253 species containing covalently bound CNC. In order to exclude the possibility that such peaks are due to CNC
254 themselves, SEC analysis of CNC alone was also performed in the same experimental conditions. No signals
255 were registered, confirming that such peaks in the chromatograms of PLA-CNC can only be related to
256 nanocomposites produced by chemical reaction of CNC with lactide. In principle, further macromolecular
257 entities could be also formed from CNC and lactide, whose dimensions are larger than those of filter pores
258 used for SEC.

| SAMPLE | CNC CONTENT (%W/W) | $M_p$ (Da) |
|--------|--------------------|-----------|
| PLA | 0 | 283600 |
| PLA0.5 | 0.5 | 182400 |
| PLA2 | 2 | 110600 |
| PLA2.5 | 2.5 | 81900 |
| PLA3 | 3 | 55000 |
| PLA5 | 5 | 53500 |

**Table 2:** Peak molecular weight for synthesized nanocomposites
relative to peaks between 1400 and 1700 sec.
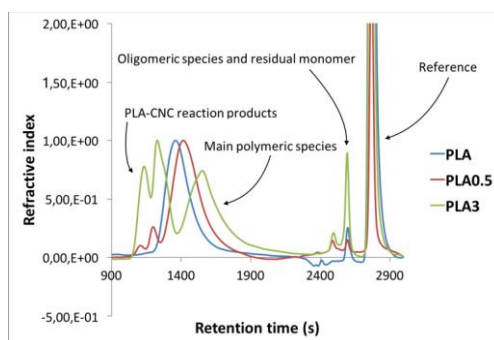
265
266
267

**Figure 1:** SEC graphs for PLA, PLA0.5 and PLA3 samples.

268
269 **Thermal analyses (DSC)**
270 **Figure 2** reports the second heating scan for DSC thermograms of all samples, compared to the thermogram
271 of standard PLA. All samples show similar behavior. Indeed, after the first heating cycle necessary to eliminate
272 residual internal stresses deriving from the synthesis, they do not crystallize during cooling. Crystallization
273 occurs during the second heating (cold crystallization), affording a crystalline phase which is characterized by
274 two melting peaks. It can be noted that the peak at lower temperature becomes more intense as the wt.%
275 of CNC increases. It is well known[28, 29] that PLA can crystallize in three different forms, depending on the
276 crystallization conditions, namely α, β and ϒ forms. Crystallization from the melt above 120 °C results in the
277 formation of stable crystals labeled as α-crystals. They are characterized by the packing of two chain
278 segments with a $10_3$ helical conformation to form an orthorhombic unit cell. The α-form is the most common
279 PLA crystalline phase, while β and ϒ ones form through different thermal/mechanical treatments.
280 It has been demonstrated[30, 31] that, when crystallization from the melt occurs with isothermal analyses at
281 temperatures lower than 120 °C, the formation of more disordered and metastable α'-crystals is promoted.
282 Such crystals show slightly larger unit-cell dimensions as well as lower packing density in comparison to α-
283 crystals. Their existence can explain the splitting of melting peaks in PLA, observed also in previous
284 literature.[32]
285 Coming to our DSC experiment, the high regularity of the chains in the standard PLA sample leads to the
286 formation of α-crystals during cold crystallization, resulting in a single melting peak, bearing a slight shoulder
287 at lower temperature, probably due to a small presence of α'-crystals. When CNC are added in the
288 polymerization feed, giving rise to *in situ* polymerization with lactide, they probably lead to more disordered
289 crystals, with the melting peak at lower temperature becoming more and more evident as CNC wt.%
290 increases. This seems to indicate that the higher is the wt.% of CNC, the more favored will be the formation
291 of α'-phase. From **Figure 2** it can also be noticed that cold crystallization temperature increases as the wt.%
292 of CNC increases.
293 Analyzing DSC data, reported in **Table 3**, it appears that CNC make crystallization of PLA more difficult.
294 Interestingly, in literature data relative to PLA-CNC blends, an opposite trend is reported, i.e. an improvement
295 in crystallization kinetics with respect to standard PLA.[33] In those cases, nanocrystals seem to have a
296 nucleating effect, favoring the formation of crystals. It appears, however, that an increase in affinity between
297 PLA and CNC (i.e. by modification through grafting approaches) leads to lower crystallization kinetics.[20, 24] In
298 particular, it was hypothesized that the greater is the adhesion of polymer chains onto nanocrystals surface,
299 the lower is the mobility for chains themselves, with consequent slowing in crystals' formation.
300 In our nanocomposites, CNCs act presumably as disturbing agents for crystallization since the chemical
301 anchoring onto nanocrystals surface brings to a decrease of the degrees of freedom for polymeric chains.
302 This eventually leads to a more difficult organization of macromolecules and, therefore, to a more difficult
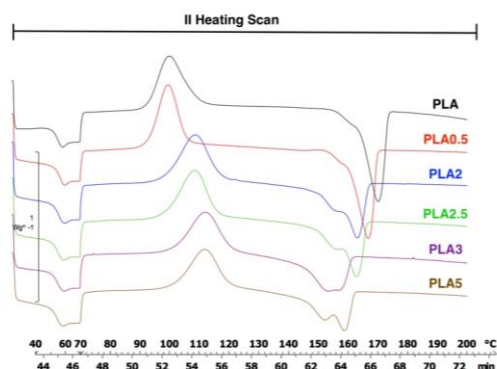303 formation of crystals.
304

**Figure 2:** DSC thermograms for all samples.

| Sample | $T_g$ (°C) | $T_{CC}$ (°C) | $T_m$ (°C) |
|--------|-----------|---------------|------------|
| PLA | 54 | 100 | 170 |
| PLA0.5 | 53 | 99 | 166 |
| PLA2 | 54 | 109 | 163 |
| PLA2.5 | 54 | 108 | 163 |
| PLA3 | 54 | 112 | 157 |
| PLA5 | 53 | 112 | 159 |

**Table 3:** thermal DSC data for all samples

**Thermal analyses (TGA)**

**Figure 3** shows TGA curves of all PLA-CNC nanocomposites. All samples show a single step degradation pathway. Thermal stabilities of PLA nanocomposites were evaluated from TGA thermograms checking temperatures corresponding to 5%, 30%, 50% and 95% of weight loss ($T_{5\%}$, $T_{30\%}$, $T_{50\%}$ and $T_{95\%}$ respectively). It has to be pointed out that all nanocomposites show higher thermal stability in comparison to standard PLA. This result marks an important difference from what reported for PLA-CNC nanocomposites obtained via compounding, for which a decrease, or in the best cases no variations in thermal stability in comparison to PLA are detected.[18, 19] It must be considered that CNC are routinely obtained through $H_2SO_4$-based hydrolysis of cellulose fibers and they are therefore recovered bearing sulfate groups. It is reported that thermal stability of CNC is strongly related to the acidity of the sulfate groups on the crystals surface,[17, 34, 35] i.e. the higher is the quantity of sulfate groups, the easier is expected to be the thermal degradation. Most likely, this is the reason also for the observed enhanced thermal degradation in the case of physical mixtures between PLA and CNC.

Functionalization of CNC with different moieties has been explored, in order to obtain a higher thermal stability of crystals themselves and, in turn, of resulting nanocomposites.[20] In almost all reported cases, however, no improvements were registered for what regards the thermal stability of the materials obtained. An increase of thermal degradation temperature (around 12 °C in the best case) was reported by Dhar and co-workers, when the reactive extrusion process was adopted (see Introduction).[25] In this latter case $T_{onset}$ increased of about 12 °C and $T_{50\%}$ of around 5 °C.

As shown by the data reported in **Table 4**, all PLA-CNC samples show higher degradation temperatures with respect to standard PLA. Among reported data, $T_{5\%}$, corresponding to 5% weight loss, can be considered as the starting point for thermal degradation. It appears that all nanocomposites show improved thermal resistance, with $T_{5\%}$ that increases up to 25 °C in the best case in comparison to standard PLA. The difference in weight loss between standard PLA and nanocomposites becomes less pronounced with the increase of

344 temperature. It has to be said, however, that all CNC containing samples appear to possess higher $T_{30\%}$ (up
345 to ~25 °C) and higher $T_{50\%}$ (up to ~14 °C), indicating a marked improvement over best previous literature
346 results.
347 The improvement of thermal stability for nanocomposites can be hypothetically ascribed to two factors.
348 From one side it is reasonable to think that reaction between CNC and L-lactide allows to "mask" the
349 deleterious sulfate groups that otherwise would increase thermal degradation.
350 Secondly, it is possible that, the reduced mobility of chains due to their linkage to nanocrystals allows a better
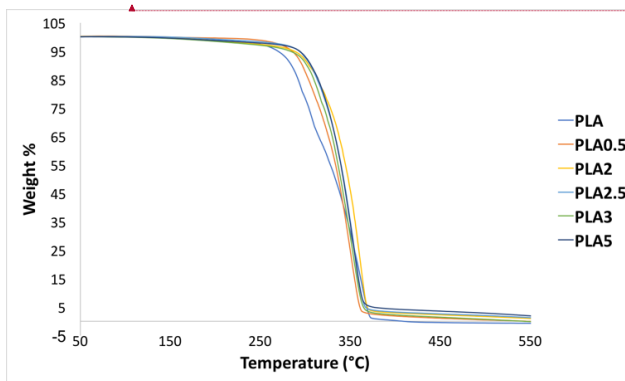351 thermal stability, making chains stiffer and less prone to oxidation and degradation reactions.

| SAMPLE | $T_{5\%}$ (°C) | $T_{30\%}$ (°C) | $T_{50\%}$ (°C) | $T_{95\%}$ (°C) |
|--------|--------|--------|--------|--------|
| PLA | 262 | 301 | 325 | 360 |
| PLA0.5 | 279 | 314 | 330 | 353 |
| PLA2 | 281 | 325 | 340 | 361 |
| PLA2.5 | 286 | 322 | 335 | 359 |
| PLA3 | 282 | 320 | 332 | 358 |
| PLA5 | 286 | 322 | 335 | 366 |

**Table 4:** Thermal degradation temperatures corresponding to defined weight losses for all samples.



**Figure 3:** TGA curves for all samples.

368 **Rheological analyses**

369 Since the reinforcing effect of CNC in PLA matrices is well known,[36, 37] we performed rheological analyses, in
370 order to evaluate the effect of the *in situ* polymerization protocol on the complex viscosity and storage
371 modulus. As the wt.% of CNC increases, two effects can be observed. From one side, the high rigidity of CNC
372 contributes to increase the melt viscosity. This trend is in contrast with the related decrease in molecular
373 weight of the PLA polymer, observed by SEC, that acts in the opposite direction, lowering the melt viscosity.
374 Rheological curves obtained via frequency sweep experiments are reported in **Figure 4** for all samples.
375 Sample PLA0.5 shows viscoelastic behavior with a Newtonian plateau at low shear rates and a shear thinning
376 behavior. PLA sample shows a decrease in viscosity at low shear rates, caused by partial degradation of the
377 sample during the analysis: in PLA0.5 such effect is not visible, probably thanks to the thermal stabilizing
378 effect of CNC, as explained in TGA paragraph. Although all materials behave as thermoplastics, with the
379 increase of wt.% CNC samples tends to have an increased shear sensitivity in all range of frequencies. This
380 behavior is marked for PLA 2 and PLA3 samples.
381 Storage (G') modulus curves (**Figure 5**) show that PLA sample has the typical behavior of a thermoplastic
382 polymer, with the low shear zone slope of G' curve being around 2. With the increase of CNC wt.%, the slope
383 of the curve becomes significantly lower and the whole G' plot tends to a straight line. A trend of this type
384 can be attributed to the progressive transition from liquid- to solid-like behavior, which therefore indicates
385 a good dispersion of nanoparticles into the polymeric matrix. As expected, PLA0.5 shows the smallest
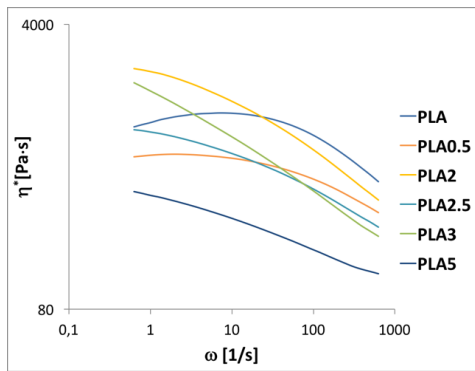386 difference with standard PLA.
387



388
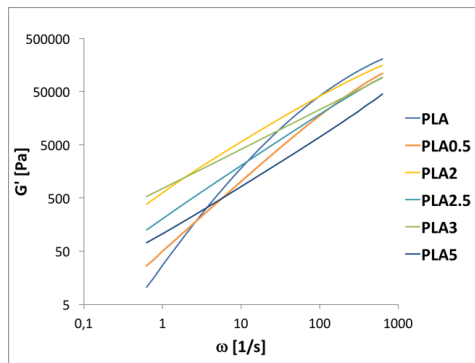389 **Figure 4:** complex viscosity curves for all samples.



390
391 **Figure 5:** storage modulus curves for all samples.

392

| Sample | G' [Pa] | |
|---|---|---|
| | at $\omega$ = 628.3 s$^{-1}$ | at $\omega$ = 0.6823 s$^{-1}$ |

| | | |
|---|---|---|
| PLA | 205800 | 10 |
| PLA0.5 | 110300 | 26 |
| PLA2 | 154600 | 381 |
| PLA2.5 | 92950 | 126 |
| PLA3 | 90490 | 537 |
| PLA5 | 45380 | 72 |

**Table 5:** storage modulus values at the two extremes of the curves.

In **Table 5** storage modulus values at $\omega$ = 628.3 s$^{-1}$ and at $\omega$ = 0.6823 s$^{-1}$, which are the extremes of the curves, are reported. The trend just described is here well highlighted, with PLA sample that shows the highest G' at high frequency and the lowest at low frequency, while all nanocomposites show a less pronounced decrease of storage modulus values.

**WAXS Analyses**

Crystalline structure of PLA and PLA-CNC nanocomposites was studied through WAXS analyses on films obtained by casting from a PLA solution in CHCl$_3$ as previously described. As **Figure 6** shows, PLA sample appears to have four characteristic peaks at $2\theta$ = 14.60°, 16.68°, 19.14° and 22.27°, as already reported in literature.[38] Crystallinity of PLA0.5 sample seems to be not significantly affected by the presence of cellulose nanocrystals. As concentration of CNC increases, however, the crystallinity of nanocomposites decreases. In the case of PLA2 signals relative to PLA are still present. However they are less sharp and the peak at 22.27° is barely appreciable. An additional increase of concentration (namely PLA2.5, PLA3 and PLA5 samples) brings to a further decreased of crystallinity. These three nanocomposites show a broad peak centered around $2\theta$ = 16° and characteristic PLA peaks are not detectable anymore. Interestingly, however, it should be noted that with the increase in w/w% of CNC, the crystalline peak of PLA shifts towards lower values of $2\theta$. To this regard, it is well known in literature that the peak at $2\theta$ = 16.7° is relative to $\alpha$ crystalline phase of PLA.[16] This signal shifts as the contribution of $\alpha'$ form becomes higher, reaching values equal to $2\theta$ = 16.4°.[39, 40] As **Figure 6** shows, all nanocomposites with except of PLA0.5, show lower values of $2\theta$ in this spectral region, therefore confirming DSC data regarding the presence of differently ordered crystalline phases.

In addition, it appears that for samples with the highest concentrations of CNC, the signals pattern of nanocrystals becomes more and more evident. As shown in **Figure 7**, CNC show four main peaks at $2\theta$ = 14.79°, 16.58°, 22.83° and 45.23°. The peak at $2\theta$ = 32° is spurious and presumably related to K$_2$SO$_4$ generated during the extraction of nanocrystals. Meanwhile the two peaks at 14.79° and 16.58° respectively cannot be detected under the broad signal in PLA2.5, PLA3 and PLA5 samples. It appears that the other two peaks appear with increasing intensity as the concentration of CNC increases in the material. In particular, for what regards PLA5, both a shoulder around 22.5° and a peak around 54.5° are present, closely resembling signals relative to pure CNC. It is therefore reasonable to think that at high concentration of CNC the dispersion of nanocrystals in the matrix becomes less efficient, leading to the presence of some CNC crystalline domains.
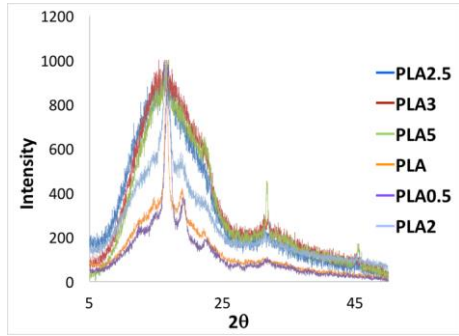
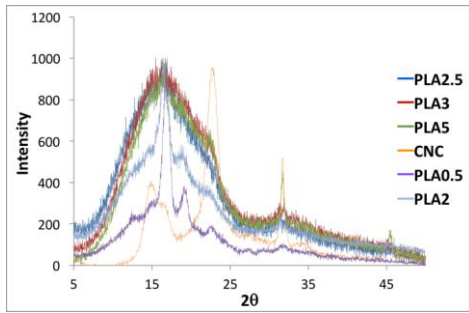**Figure 6:** WAXS diffractograms for all nanocomposites and PLA sample.



**Figure 7:** WAXS diffractograms for all nanocomposites and CNC sample.

## TEM analyses

The dimensions of cellulose nanocrystals used for the preparation of nanocomposites were determined via TEM. In **Figure 8** a TEM image of CNC is reported.
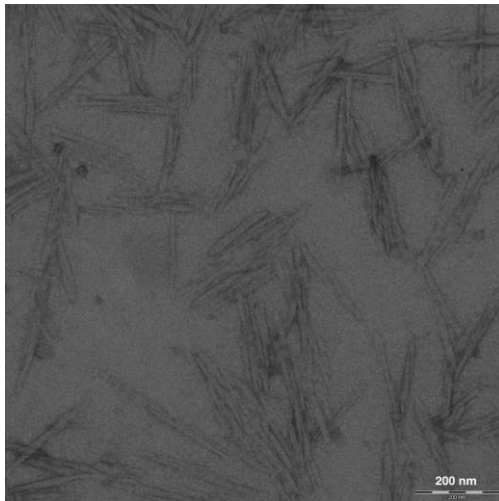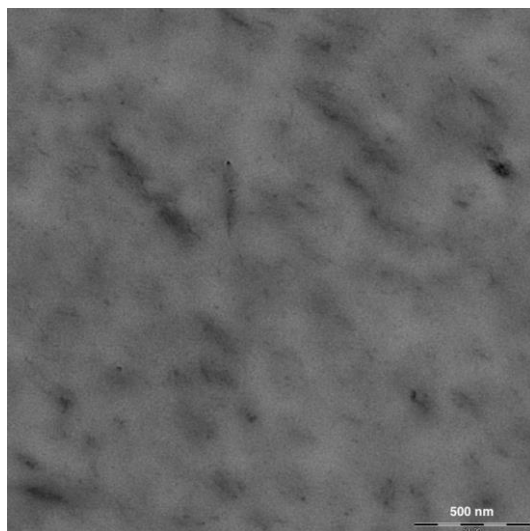


**Figure 8:** TEM micrograph of CNC.

437  Cellulose nanocrystals have an average length of $195 \pm 28$ nm and an average diameter of $16 \pm 4$ nm, resulting
438  in an aspect ratio of $13 \pm 4$.
439  In **Figure 9** a TEM micrograph of PLA5 is reported. PLA5 was chosen because it is the sample having the higher
440  content of CNC among all nanocomposites samples. In **Figure 9**, CNC can be distinguished over the polymeric
441  matrix as randomly distributed dark halos.
442



**Figure 9:** TEM micrograph of PLA5 sample.

445  CNC are not clearly different from the polymeric matrix, differently from what reported for CNC-PLA blends.[41]
446  Such difference can be ascribed to the scarce affinity between CNC and PLA in classical blends, which results
447  in a distinct separation of the two phases. In our case, the *in situ* growth of PLA chains onto CNC surface
448  allows the crystals to be fully embedded in the polymer, with an intimate interfacial contact.
449  It is also important to note that crystals' dimensions in PLA5 appear to be of the same order of magnitude as
450  in CNC alone, even if dimensions cannot be accurately determined because of the indefinite profile of
451  dispersed crystals. Again, this result underlines a clear morphological difference between nanocomposites
452  here described and PLA-CNC blends, in which the formation of CNC agglomerates is reported.[42] The uniform
453  dispersion within the polymeric matrix is another proof of the efficacy of the *in situ* approach for the
454  preparation of PLA-CNC nanocomposites even at relatively high loadings of CNC.
455
456  **FT-IR and $^1$H NMR analyses**
457  In PLA FT-IR spectrum the peak relative to ester carbonyl groups can be recognized at 1747 cm$^{-1}$, as well as
458  signals between 1000 and 1200 cm$^{-1}$ can be ascribed to C-O bonds in aliphatic esters. CNC spectrum is
459  characterized by the presence of a strong signal at 3335 cm$^{-1}$ that can be attributed to the free OH groups on
460  crystals surface. The intense band at 1032 cm$^{-1}$ can be attributed to C-O ether bonds in cellulose.
461  Nanocomposites spectra closely resemble the standard PLA spectrum although some typical CNC peaks are
462  however visible. The hypothesis is that PLA chains fully cover the CNC surface, preventing most of typical
463  cellulose signals to be detected.
464  $^1$H NMR analyses show no significant differences between the spectra of PLA and nanocomposites, with the
465  presence of a quartet signal centered at 5.18 ppm, relative to hydrogen in $\alpha$ position with respect to the
466  carbonyl group and a doublet signal centered at 1.60 ppm relative to the methyl group.
467
468
469  **Conclusions**

470 In this work, cellulose nanocrystals were successfully synthesized, starting from cotton linters through acidic
471 hydrolysis, and they were subsequently used for *in situ* melt polymerization of PLA.
472 Full characterization of nanocomposites has been performed, aimed to investigate the effect of CNC on the
473 morphological and thermo-mechanical properties of materials.
474 Through SEC analysis it has been possible to assess the actual occurrence of chemical bonds between CNC
475 and PLA chains. Indeed, as the quantity of added CNC increases, the molecular weight of the polymer
476 decreases, possibly indicating a role of free OH groups on cellulose surface, as initiators during the *in situ*
477 polymerization process.
478 DSC analyses were performed to evaluate the thermal behavior of the materials. The presence of CNC in the
479 reaction system seems to favor the formation of α' crystals, which are less ordered with respect to the more
480 common α crystal form in PLA. Again, it can be argued that free OH groups act as initiators, perhaps forming
481 complex star-like macromolecular architectures which are more prone to form less ordered crystals.
482 From TGA analyses it has been clearly demonstrated that synthesized bionanocomposites show a marked
483 improvement in thermal stability with respect to standard PLA. Results indicate an improvement also with
484 respect to literature data regarding the thermal stability of various types of PLA-CNC nanocomposites.
485 Finally, nanocomposites show an improvement in rheological properties with respect to standard PLA. In
486 particular it has been shown that storage modulus markedly increases in the presence of CNC, indicating a
487 reinforcing effect given by these species.
488 In conclusion, the described *in situ* synthetic methodology allows not only an optimal compatibilization
489 between the two entities, facing one of the major problems inherent to the preparation of nanocomposites,
490 but also leads to remarkably improved thermal and rheological properties of the obtained materials, with
491 respect to standard PLA and conventional PLA-CNC nanocomposites. Among tested CNC concentrations, the
492 2 %w/w appeared to be the most promising. In fact, while TGA data remain very similar for all
493 nanocomposites, PLA2 sample proved to possess the best rheological properties, probably thanks to a
494 combination of high molecular weight and reinforcing effect given by CNC.
495

## Notes and references

497  1  Inkinen, S.; Hakkarainen, M.; Albertsson, A.; Sodegard, A.; *Biomacromolecules*; 2011; **12**; 523-532.
498  2  Datta, R.; Henry, M.; *J. Chem. Technol.* Biotechnol; 2006; **81**; 1119-1129.
499  3  Armentano, I.; Bitinis, N.; Fortunati, E.; Mattioli, S.; Rescignano, N.; Verdejo, R.; Lopez-Manchado, M.A.; Kenny, J.M.;
500     *Progress in Polymer Science*; 2013; **38**; 1720-1747.
501  4  Lunt, J.; *Polymer Degradation and Stability*; 1998; **59**; 145-152.
502  5  Auras, R.; Harte, B.; Selke, S.; *Macromol. Biosci.*; 2004; 835-864.
503  6  Raquez, J.M.; Habibi, Y.; Murariu, M.; Dubois, P.; *Progress in Polymer Science*; 2013; **38**; 1504-1542.
504  7  Ramontja, J.; Sinha Ray, S.; Pillai, S.K.; Luyt, A.S.; *Macromol. Mater. Eng.*; 2009; **294**; 839-846.
505  8  Kaseem, M; Hamad, K; Deri, F; Gun Ko, Y; *Polym. Bull.*; 2016.
506  9  Sabatini, V.; Farina, H.; Basilissi, L.; Di Silvestro, G.; Ortenzi, M.A.; *Journal of Nanomaterials*; 2015; 1-16.
507  10  Castiello,S.; Coltelli, M.B.; Conzatti, L.; Bronco, S.; *Journal of Applied Polymer Science;* 2012; **125**; E413-E428.
508  11  Basilissi, L.; Di Silvestro, G.; Farina, H; Ortenzi, M.A.; *J. App. Polym. Sci.*; 2013; 1575-1582.
509  12  Ortenzi, M.A.; Basilissi, L.; Farina, H.; Di Silvestro, G.; Piergiovanni, L.; Mascheroni, E.; *European Polymer Journal*; 2015; **66**;
510     478-491.
511  13  Ioelovich, M.; *BioResources*; 2008; **3**; 1403-1418.
512  14  Trache, D; Hazwan Hussin, M.; Mohamad Haafiz, M. K.; Kumar Thakur, V.; *Nanoscale*; 2017.
513  15  Mascheroni, E.; Rampazzo, R.; Ortenzi, M. A.; Piva, G.; Bonetti, S.; Piergiovanni, L.; *Cellulose*; 2016; **23**; 779-793.
514  16  Dhar, P.; Tarafder, D.; Kumar, A.; Katiyar, V.; *RSC Adv.*; 2015; **5**; 60426-60440.
515  17  Ambrosio-Martin, J.; Fabra, M. J.; Lopez-Rubio, A.; Lagaron, J. M.; *Cellulose*; 2015; **22**; 1201-1226.
516  18  Pracella, M.; Minhaz-Ul Haque, Md.; Puglia, D.; *Polymer*; 2014; **55**; 3720-3728.
517  19  Spinella, S.; Lo Re, G.; Liu, B.; Dorgan, J.; Habibi, Y.; Leclere, P.; Raquez, J. M.; Dubois, P.; Gross, R. A.; *Polymer*; 2015; **65**; 9
518  20  Bledzki, A. K.; Gassan, J.; *Prog. Polym. Sci.*; 1999; **24**; 221-274.
519  21  Lizundia, E.; Fortunati, E; Dominici, F; Vilas, J. L.; Leon, L. M.; Armentano, I.; Torre, L.; Kenny, J. M.; *Carbohydrate
520     Polymers*; 2016; **142**; 105-113.
521  22  Mujica-Garcia, A.; Hooshmand, S.; Skrifvars, M.; Kenny, J. M.; Oksman, K.; Peponi, L.; *RCS Adv.*; 2016; **6**; 9221-9231.
522  23  Goffin, A. L.; Raquez, J. M.; Duquesne, E.; Siqueira, G.; Habibi, Y.; Dufresne, A.; Dubois, P.; *Biomacromolecules*; 2011; **12**;
523     2456-2465.
524  24  Dhar, P.; Tarafder, D.; Kumar, A.; Katiyar, V.; *Polymer*; 2016; **87**; 268-282.
525  25  Yang, W.; Dominici, F.; Fortunati, E.; Kenny, J.M.; Puglia, D.; *RSC Adv.*; 2015; **5**; 32350-32357.

526  26  Nakayama, N; Hayashi, T.; *Polymer degradation and stability*; 2007; **92**; 1255-1264.
527  27  Kaewprapan, K.; Phattanarudee, S.; *J. Nanosci. Nanotechnol.*; 2012; **12**; 781-786.
528  28  Kawai, T.; Rahman, N.; Matsuba, G.; Nishida, K.; Kanaya, T.; Nakano, M.; Okamoto, H.; Kawada, J.; Usuki, A.; Honma, N.;
529      Nakajima, K.; Matsuda, M.; *Macromolecules*; 2007; **40**; 9463-9469.
530  29  Cocca, M.; Di Lorenzo, M. L.; Malinconico, M.; Frezza, V.; *European Polymer Journal*; 2011; **47**; 1073-1080.
531  30  Righetti, M. C.; Gazzano, M.; Di Lorenzo, M. L.; Androsch, R.; *European Polymer Journal*; 2015; **70**; 215-220.
532  31  Zhang, J.; Tashiro, K.; Tsuji, H.; Domb, A. J.; *Macromolecules*; 2008; **41**; 1352-1357.
533  32  Di Lorenzo, M. L.; Androsch, R.; *Macromol. Chem. Phys.*; 2016.
534  33  Gardebjer, S.; Bergstrand, A.; Idstrom, A.; Borstell, C.; Naana, S.; Nordstierna, L.; Larsson, A.; *Composites Science and*
535      *Technology*; 2015; **107**; 1-9.
536  34  Lu, P.; Hsieh, Y. L.; *Carbohydrate Polymers*; 2010; **82**; 329-336.
537  35  Roman, M.; Winter, W. T.; *Biomacromolecules*; 2004; **5**; 1671-1677.
538  36  Bagheriasl, D.; Carreau, P. J.; Riedl, B.; Dubois, C.; Hamad, W. Y.; *Cellulose*; 2016; **23**; 1885-1897.
539  37  Kamal, M. R.; Khoshkava, V.; *Carbohydrate Polymers*; 2015; **123**; 105-114.
540  38  Ki, W. K.; Seong, I. W.; *Macromol. Chem. Phys.*; 2002; **203**; 2245.
541  39  Marubayashi, H.; Akaishi, S.; Akasaka, S.; Asai, S.; Sumita, M.; *Macromolecules*; 2008; **41**; 9192-9203.
542  40  Zhang, J.; Duan, Y.; Sato, H.; Tsuji, H.; Noda, I.; Yan, S.; Ozaki, Y.; *Macromolecules*; 2005; **38**; 8012-8021.
543  41  Sanchez-Garcia, M.D.; Lagaron, J.M.; *Cellulose*; 2010; **17**; 987-1004.
544  42  Gupta, A.; Simmons, W.; Schueneman, G.T.; Hylton, D.; Mintz, E.A.; *ACS Sustainable Chem. Eng.*; 2017; **5**; 1711-1720.